IEEE Access
Multidisciplinary | Rapid Review | Open Access Journal

Received August 28, 2020, accepted September 6, 2020, date of publication September 14, 2020,
date of current version September 24, 2020.

Digital Object Identifier 10.1109/ACCESS.2020.3023672

Liquid-Metal Nodal Sheet for Reconfigurable Devices and Circuits

KAREEM S. ELASSY[1,2], (Student Member, IEEE), M ARIFUR RAHMAN[1], (Senior Member, IEEE), WAYNE A. SHIROMA[1], (Senior Member, IEEE), AND AARON T. OHTA[1], (Senior Member, IEEE)

[1]Department of Electrical Engineering, University of Hawai'i at Mānoa, Honolulu, HI 96822, USA
[2]Center of Excellence, Arab Academy for Science, Technology and Maritime Transport, Cairo 12577, Egypt

Corresponding author: Aaron T. Ohta (aohta@hawaii.edu)

This work was supported in part by the U.S. Defense Advanced Research Projects Agency under Grant W31P4Q-16-1-0005.

ABSTRACT Gallium-based liquid metals have attracted attention as a conductive adaptable material that can be shaped to obtain reconfigurability. We demonstrate a two-dimensional array of liquid-metal conductive nodes, in which reconfigurability is achieved by merging and splitting adjacent nodes to reversibly shape a two-dimensional structure. The nodes are reconfigured using three different actuation schemes: 1) pressure-point actuation, where the liquid metal is actuated by pressing on the flexible superstrate; 2) surface-tension self-splitting, where the geometric shape of the node itself exerts a separating force on merged nodes; and 3) electrocapillary actuation where the liquid metal is actuated by a DC electrical signal. This is the first demonstration of a reconfigurable liquid-metal pixel array using liquid-liquid interconnects for prototyping reconfigurable devices. As a proof of concept, the proposed actuation techniques are used to reconfigure a liquid-metal nodal patch antenna, in which the liquid-metal nodes are reversibly connected and disconnected to change the operating frequency and polarization.

INDEX TERMS Liquid metal, reconfigurable antenna, electrocapillary actuation, Galinstan.

I. INTRODUCTION

A reconfigurable system can be reversibly tuned, reshaped, or altered to fulfill a changing objective, and can be classified into various domains such as acoustic, electromagnetic, electronic, fluidic, magnetic, mechanical, photonic, and thermal [1]. The electronic domain can be further divided into digital and analog, with the analog subdomain further subdivided into RF, small-signal, and power [1]. To the best of our knowledge, this is the first paper merging the fluidic and RF reconfigurable domains using the concept of pixelated liquid metal employing liquid-liquid metal interconnects.

An example of a reconfigurable RF component is a phase shifter consisting of multiple, isolated transmission lines with interconnecting switches, which when turned on or off, can increase or decrease the overall length of the line. Reconfigurability is not limited to just one dimension, however. An example of a two-dimensional reconfigurability scheme is shown in Fig. 1, illustrating a pixelated grid of isolated metal nodes that can be connected or disconnected as desired to create various shapes, mimicking a reconfigurable Etch-a-Sketch-like surface.

The associate editor coordinating the review of this manuscript and approving it for publication was Chan Hwang See.

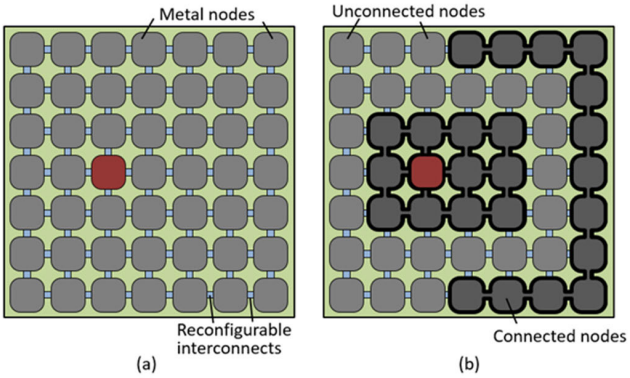

FIGURE 1. Notional example of a reconfigurable microcircuit, showing metal nodes that are: (a) unconnected, and (b) connected to form a patch antenna with a parasitic resonant structure. The red node is connected to an RF feed from below, and selected nodes are connected via reconfigurable interconnects.

The advantage of such a shape-shifting reconfigurable RF system is the ability to adjust parameters such as operating frequency, power, and radiation pattern to optimize performance in a dynamically changing environment.

This pixelation scheme has been successfully implemented for reconfigurable antennas, in which the fixed conductive

elements are connected or disconnected by interconnecting switches [2]–[4]. However, these antennas are subject to inherent scaling issues due to the large number of switches required, and their performance is therefore limited by the insertion loss introduced by these switches. In short, the same switches which enable this reconfiguration scheme are also the limiting factor for this scheme. In fact, reconfigurable antennas in general – not just pixelated ones – are essentially a set of passive structures infused with switches [1], so the performance of large arrays is limited by the switches themselves.

In the past few years, liquid metal has emerged as a method for reconfiguring various RF components such as filters, switches, and antennas [5]–[9]. One type of liquid metal is Galinstan (Geratherm Medical AG), an alloy of gallium, indium and tin that is liquid at room temperature, has good electrical conductivity (3.4×10^6 S/m) [10], and can be actuated both hydraulically [11], [12] and electrically [13], [14]. By replacing the pixelated conductive elements in Fig. 1 with liquid metal, a reconfigurable microcircuit can be realized without the limiting factor of switches. The metastable merging of adjacent liquid-metal elements not only removes the aggregate insertion loss of (potentially) hundreds of switches, but also opens the door to more complex circuits, such as larger arrays, by making the technology scalable. This merging is reversible, and is accomplished via low-voltage, low-power electrical signals which need not be continuously applied to maintain an actuated or unactuated state.

The first demonstration of pixelated liquid metal involved electrically actuating Galinstan to fill or evacuate selected pixels [15], [16]. Although these demonstrations were single-pixel and 4-pixel proof-of-concept prototypes with no circuit functionality, Fig. 2 shows the general idea. Compared to Fig. 1, where isolated metal pixels always exist on the surface and the reconfiguration mechanism is the interconnection between those pixels, Fig. 2 shows that the default state is empty pixels devoid of metal [Fig. 2(a)], and the reconfiguration mechanism involves filling or evacuating pixels with liquid metal [Fig. 2(b)]. Although novel in its approach, this scheme requires solid-metal connectors between pixels to maintain inter-pixel connectivity, as well as a buried liquid-metal reservoir.

Each pixel-pixel interconnection involves a liquid-solid-liquid interface due to the solid-metal connectors, which not only results in small but non-zero parasitic effects, but the solid metal must be carefully selected to avoid undesired alloying effects. In [10], pixel-pixel interconnections were implemented with stainless steel, which prevents alloying but does not have a high electrical conductivity. To circumvent the issues associated with liquid metal contacting solid metal, electrical connections between two discrete volumes of liquid metal can be implemented [17], [18].

This article demonstrates the first liquid-metal pixel array using liquid-liquid interconnects for prototyping reconfigurable devices. We demonstrate a two-dimensional array of liquid-metal nodes, called a liquid-metal nodal sheet, that can be reshaped through merging and splitting of the nodes. Compared to the out-of-plane actuation method of [16], the fabrication is simpler as there are no pre-existing connections between nodes nor sub-layer reservoirs. No cleanroom processes were used for fabrication, unlike [17] and [18]. As a proof-of-concept, we demonstrate that the liquid-metal nodal sheet can implement a patch antenna that has reconfigurable operating frequency and polarization. Using liquid-liquid interconnects achieves an objective for pixelated antennas stated in [1], in which "contiguous pixels are designed to coalesce into conductive islands."

II. CONCEPT

Fig. 3 illustrates the liquid-metal nodal sheet concept, using a 2×2 array for simplicity. Each liquid-metal-filled, diamond-shaped node is 1 cm $\times$ 1 cm, with adjacent nodes intersecting at their corners; this overlapping area is the liquid-metal merging and splitting point for adjacent

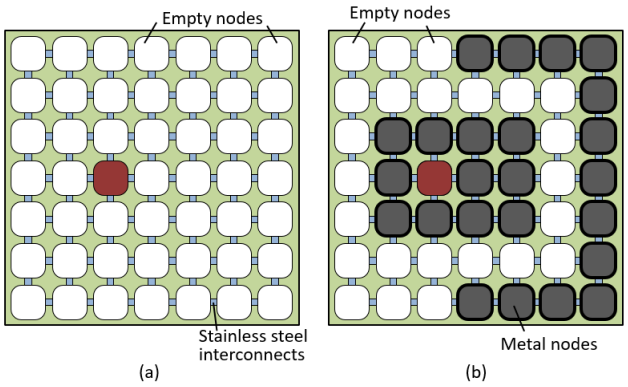

FIGURE 2. Compared to Fig. 1, an alternative pixelation scheme showing empty pixels that are: (a) unfilled, and (b) partially filled with liquid metal to form a patch antenna with a parasitic resonant structure.

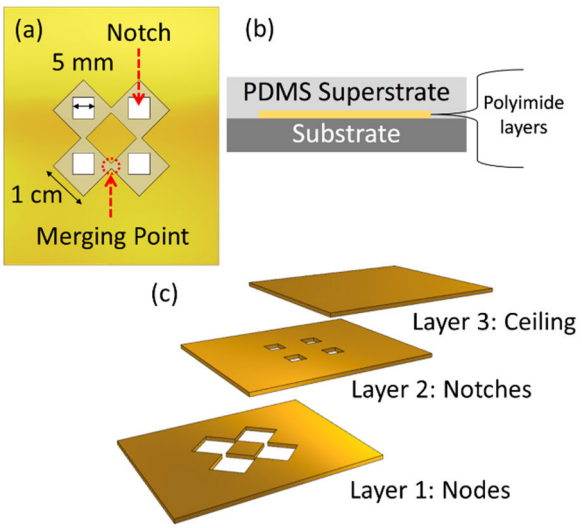

FIGURE 3. Nodal sheet concept: a) top view of nodal sheet geometry; b) cross section; c) polyimide layer stack.

nodes [Fig. 3(a)]. The nodal sheet consists of a three-layer polyimide stack sandwiched between a 1.28-mm-thick polystyrene substrate and a 5-mm-thick polydimethylsiloxane (PDMS) superstrate [Fig. 3(b)].

Fig. 3(c) illustrates the polyimide stack that forms the fluidic channels and nodes. The node and notch layers are fabricated from 240-μm-thick double-sided polyimide tape (PPTDE-2 Kapton), using a commercial craft cutter (Silhouette Portrait) [19]. The node layer forms the walls of the nodes. The widths of the channels connecting adjacent nodes range from 0.5 mm to 2.5 mm; the effect of changing the channel width is explained in more detail in Section III.B. The notch layer, consisting of 5 mm $\times$ 5 mm square notches centered above each node, enables metastable locking [20], localizing the liquid metal at the center of each node while allowing it to merge with neighboring nodes without transferring its entire volume. The symmetric notch shape allows the liquid metal to move isotropically to surrounding nodes. The ceiling layer is made of 80-μm-thick polyimide and serves as a cap for the other layers, while providing good adhesion with the 5-mm-thick, optically transparent PDMS superstrate.

The nodes are first filled with an electrolytic solution of 1-M sodium hydroxide (NaOH) solution that prevents the Galinstan from forming an oxide layer when exposed to air [13], allowing the liquid metal to move smoothly inside the nodes. Each node is then filled separately with Galinstan using a 30-gauge needle. The elasticity of the PDMS superstrate allows it to self-heal after injecting the NaOH and Galinstan.

III. LIQUID-METAL ACTUATION SCHEMES

The liquid-metal nodes can be merged and split using three different actuation schemes: 1) pressure-point actuation, where the liquid metal is actuated by pressing on the encapsulating PDMS; 2) surface-tension self-splitting, where the geometric shape of the node itself exerts a separating force on merged nodes; and 3) electrocapillary actuation (ECA), where the liquid metal is actuated by a DC electrical signal [14], [21]. It is also possible to use combinations of these actuation schemes to merge and split the nodes depending on the actuation force used. Fig. 4 shows the forces associated with merging and splitting the nodes which facilitates the following discussion of the three actuation schemes. Here, the surface-tension notch force F_{notch} points from the center of mass of the liquid metal to the top of the notch, and the merged liquid-metal surface-tension force $F_{merging}$ points from the center of mass to the merging point.

A. PRESSURE-POINT MERGING AND SPLITTING

The pressure-point scheme of merging and splitting liquid-metal nodes involves pressing on the nodes and at the intersections of two adjacent nodes, respectively (Figs. 5 and 6). The blunt end of a tweezer is used to apply the force on the nodes. The PDMS superstrate deforms under applied force, displacing the liquid metal. Pressing in the middle of a node extends the liquid metal to the neighboring nodes, depending

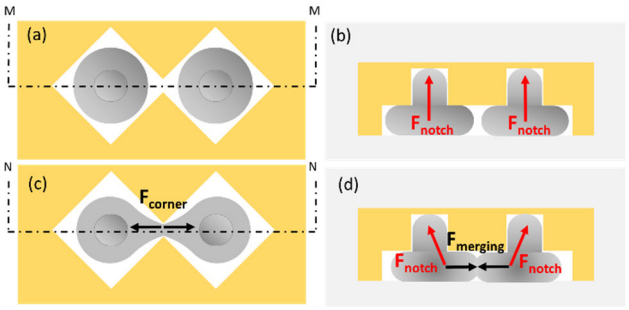

FIGURE 4. Forces associated with merging and splitting the nodes: a) top view of disconnected nodes in the form of isolated circular disks; b) cross-section view [M-M in Fig. 4(a)] for the disconnected nodes with F_{notch} pinning the liquid metal at the center of the node; c) top view of merged liquid-metal nodes; d) cross-section [N-N in Fig. 4(c)] for the connected nodes showing F_{notch} and $F_{merging}$.

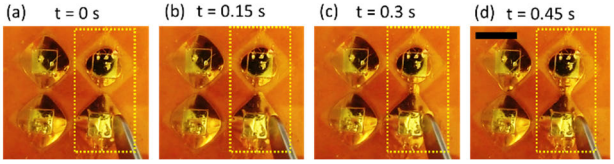

FIGURE 5. Snapshots for merging liquid-metal nodes (within the dashed outline) by pressure-point scheme in 0.45 s: a) pressing force is applied at the lower-right node; b) to c) liquid metal moves to merge with the upper-right node; d) merging is completed. Scale bar is 1 cm.

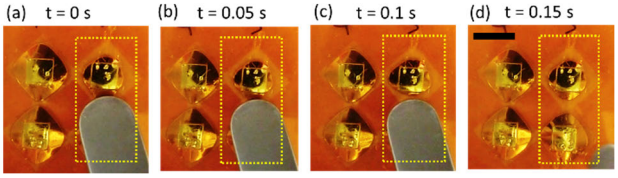

FIGURE 6. Snapshots for splitting liquid-metal nodes (within the dashed outline) by pressure-point scheme in 0.15 s: a) force is applied at the merging point between the right nodes; b) to c) liquid metal moves, splitting the merged nodes; d) splitting is completed. Scale bar is 1 cm.

on the direction of the lateral force component [Fig. 5(a)–(d)]. Consequently, the liquid metal displaces the less dense electrolytic solution at the channel and merges with the liquid metal of the adjacent node in 0.45 s. The merged nodes maintain unity in the shape of a bowtie [Fig. 5(d)] due to the high surface tension (0.535 N/m [10], [22]) of Galinstan. The surrounding NaOH suppresses the oxide layer from forming on the liquid-metal surface, thus preventing the liquid metal from sticking to the surrounding walls. To split adjacent nodes [Fig. 6(a)–(d)], pressure is exerted at the merging point of the channel, exceeding $F_{merging}$ and breaking the connection. The liquid metal recovers its geometric shape in 0.15 s, localizing at the node's center due to F_{notch}, shown in Fig. 4(b). The notch acts as a local surface-energy well where the liquid metal experiences a surface-energy minima.

B. SURFACE TENSION SELF-SPLITTING

An alternative means of disconnecting liquid-metal nodes is surface-tension-assisted self-splitting, which occurs when F_{notch} is greater than $F_{merging}$, e.g. in the case when the

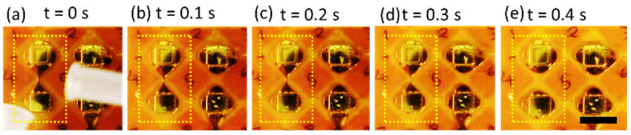

FIGURE 7. Self-splitting of liquid-metal nodes (within the dashed outline) due to surface tension in 0.4 s: a) merging force is removed; b) to d) merged liquid metal splits; e) splitting is completed. Scale bar is 1 cm.

merging force is removed (Fig. 7 and video S1). Self-splitting is facilitated by the geometric shape of the nodes; diamond-shaped nodes intersect at the corners, creating a narrow channel connecting both nodes that forces the liquid metal to occupy a smaller area, thus weakening $F_{merging}$. At the same time, F_{notch} can be increased by increasing the notch height.

A sufficiently small $F_{merging}$ allows F_{notch} to dominate and split the merged liquid metal, allowing it to retract back to the physical dimensions that satisfies minimum surface energy as illustrated in Fig. 4(d). It is essential to precisely control the liquid-metal volume at each node to enable self-splitting. The liquid-metal critical filling factor f_c is defined as the maximum volume that liquid metal can fill a node without suppressing self-splitting. Filling the nodes beyond f_c delivers enough $F_{merging}$ to maintain the node connection, even in the absence of the merging force, requiring external force to disconnect the nodes. Fig. 8 shows the measured f_c corresponding to channel widths ranging from 0.5 mm to 2.5 mm. As the channel width increases, merging two nodes becomes easier while self-splitting becomes more challenging. Thus, f_c decreases requiring less liquid metal at the nodes to passively disconnect the nodes once $F_{merging}$ is removed.

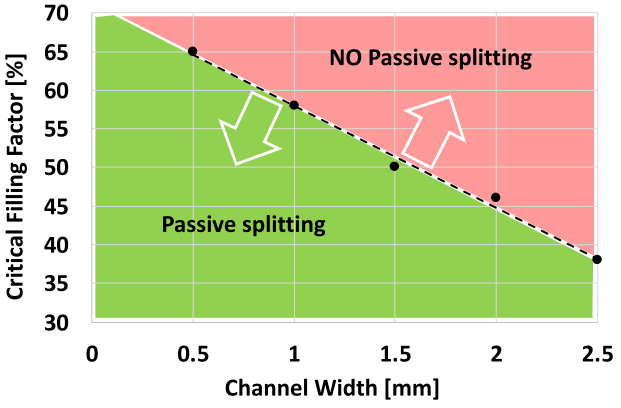

FIGURE 8. Channel width vs. liquid-metal critical filling factor f_c. The liquid-metal volume must be below f_c to enable passive splitting, otherwise liquid-metal nodes remain merged. Devices operating in the green area results in passive splitting whereas the pink area does not.

Selecting the channel width involves a tradeoff. A narrow channel width results in a larger f_c which facilitates merging, but a narrower channel also increases the likelihood of trapped air bubbles, which degrades the consistency of merging and splitting nodes. A wider channel width allows air bubbles to pass through smoothly, but the smaller f_c implies that the liquid metal needs to stretch a longer distance for merging.

C. ELECTROCAPILLARY ACTUATION (ECA)

ECA is a high-speed reversible actuation method that is capable of deforming liquid metal at rates of over 120 mm/s [14]. A low-voltage, low-power DC signal is used to induce a surface-tension gradient at the interface between the liquid metal and the surrounding electrolyte, causing the liquid metal to stretch toward the positive potential. The liquid metal immediately recovers its shape in the absence of an applied voltage to retain its minimum surface-energy state. This phenomenon is constrained by the high width-to-height ratio (30:1) of the liquid-metal channel [14]. This condition is satisfied by using a node height of 240 μm. Fig. 9(a)–(e) shows the merging of two liquid-metal nodes via ECA using 2 V DC (shown in supplementary video S2).

The PDMS superstrate is punctured at the notches with needles, which serve as electrodes to apply the actuation voltage. It takes about 1 s to merge the nodes once the ECA signal is applied (Fig. 9). Higher actuation voltages can induce faster merging. However, high voltage (above 2 V) introduces more bubbles in the device due to NaOH electrolysis; air bubbles act as a barrier for liquid-metal movement.

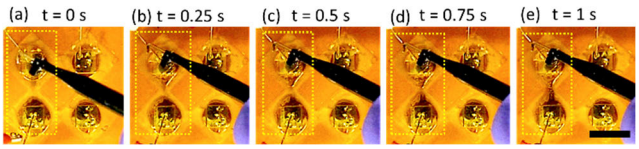

FIGURE 9. Merging liquid-metal nodes within the dashed outline) by ECA in 1 s: a) a DC voltage of 2 V is applied between the nodes; b)-d) liquid metal moves to merge the nodes; e) merging is completed. Scale bar is 1 cm.

IV. EXAMPLE APPLICATION

In this section, we present a reconfigurable liquid-metal nodal patch antenna that demonstrates switchable polarization reconfigurability by connecting/disconnecting specific nodes using the pressure-point split/merging actuation scheme.

A. EFFECT OF NODAL DISCRETIZATION OF A PATCH ANTENNA

To illustrate the usefulness of a reconfigurable liquid-metal nodal sheet, we demonstrate a liquid-metal nodal patch antenna that was implemented evolutionarily, starting from a conventional microstrip patch antenna. First, a solid copper (Cu) patch antenna was fabricated as a baseline [Fig. 10(a)(i)]. Second, a nodal Cu patch was implemented to examine the effect of diamond-shaped nodes on the antenna performance [Fig. 10(a)(ii)]. Third, the nodal Cu antenna was encapsulated with PDMS and polyimide superstrates [Fig. 10(a)(iii)] to examine their significance in the analogous end-goal liquid-metal antenna. Fourth, the Cu was replaced

TABLE 1. Comparison of measured antenna performance between 5 × 4 and 4 × 3 nodal antenna.

	5 × 4 Antenna				4 × 3 Antenna			
	Horizontal polarization				Vertical polarization			
Antenna type	**Frequency [GHz]**	**Gain [dBi]**	**Radiation eff'y (%)**	**$\|S_{11}\|$ [dB]**	**Frequency [GHz]**	**Gain [dBi]**	**Radiation eff'y (%)**	**$\|S_{11}\|$ [dB]**
Solid Cu	3.8	7.3	98	-10	3.85 (sim)	7.3 (sim)	75%	-26.63 (sim)
Nodal Cu	3.75	6.8	87	-17	3.85	5.4	4	-12.5
Nodal Cu with PDMS superstrate	3.59	6	72	-26	3.65	4.4	39	-15
Nodal liquid metal without NaOH	3.61	3.3	39	-14.3	N/A*	N/A*	N/A*	N/A*
Nodal liquid metal with NaOH	3.55	3	36	-9.9	3.6	1.3	19	-10.5

*Liquid metal nodes require the presence of NaOH for pressure-point merging/ splitting. Therefore, the 4 × 3 antenna was not examined without NaOH as it is configured from 5 × 4 in the presence of NaOH.

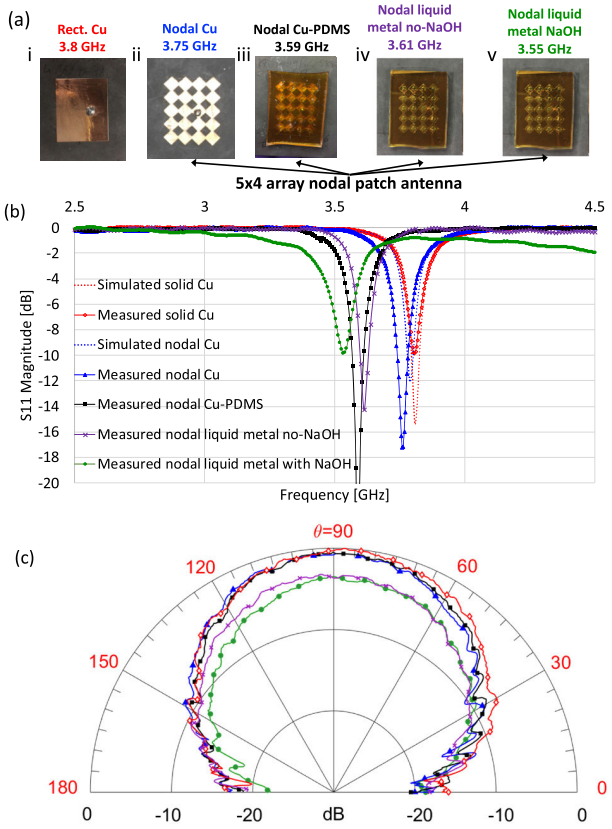

FIGURE 10. Simulated and experimental results for the different versions of solid and nodal patch antennas: a) photographs; b) simulated and measured $|S_{11}|$; c) measured radiation patterns for normalized co-polarized H-plane; the legend is the same as that in (b).

with liquid metal only (without NaOH) [Fig. 10(a)(iv)] to assess the contribution of NaOH to the losses [23] in the fifth version, which is a patch antenna that has liquid-metal nodes surrounded by NaOH to enable splitting and merging [Fig. 10(a)(v)]. All of the nodal antennas have a 5 × 4 pattern of diamond-shaped nodes [Fig. 10(a)(ii-v)]. When all of the liquid-metal nodes are connected [Fig. 10(a)(v)], the nodes form the equivalent dimensions of the solid Cu patch antenna [Fig. 10(a)(i)]. In Sec. IV.B, we describe how the liquid-metal nodes are split/merged to alter the antenna characteristics, creating a reconfigurable liquid-metal nodal patch antenna.

Rogers *Duroid* 5880 with a thickness of 0.787 mm and $\varepsilon_r = 2.2$ was used as a substrate for the antennas shown in Fig. 10(a). The solid patch antenna was designed to radiate at 3.8 GHz, according to [24]. The antenna dimensions are 31.5 mm × 25.5 mm, which is equivalent to 5 × 4 diamond-shaped nodes. Each node is 5 mm × 5 mm. The coaxial feed was positioned at the notch of a node that was located 9.35 mm from the radiating edge and 15.6 mm from the non-radiating edge. The antennas are simulated using Ansys HFSS.

The left side of Table 1 summarizes the antenna performance. Compared to the solid Cu antenna, the nodal Cu antenna has a 1% shift in resonant frequency and a 0.5 dB decrease in gain, demonstrating that nodal discretization has only a small effect on performance. The PDMS superstrate results in another 0.8 dB decrease in gain. Replacing Cu with liquid metal results in 2.7 dB gain degradation, attributed to oxide formed at liquid-metal surface; this effect was also observed in [25]. Finally, the effect of adding NaOH results in an additional 0.3 dB degradation.

B. EFFECT OF NODAL SPLITTING: POLARIZATION SWITCHING

The Cu and liquid-metal nodal patch antennas in Sec. IV.A consist of 20 interconnected node elements arranged in 5 rows and 4 columns [Fig. 10(a)(ii)]. We now describe the effect of disconnecting 1 row and 1 column of the 5 × 4 pattern, transforming it to a 4 × 3 pattern. The Cu antenna is altered by manually disconnecting specific nodes, while the liquid-metal antenna is reconfigured by pressure-point splitting. The blue and black dotted rectangles in Fig. 11(a)(i-iii) enclose the connected nodes after nodal disconnection. Three different 4 × 3 nodal antenna structures are investigated: 4 × 3 Cu, 4 × 3 Cu with PDMS superstrate, and 4 × 3 liquid metal with NaOH surrounding each node to facilitate pressure-point merging and splitting. The feed points of the 4 × 3 antennas are left unaltered from the aforementioned 5 × 4 antennas.

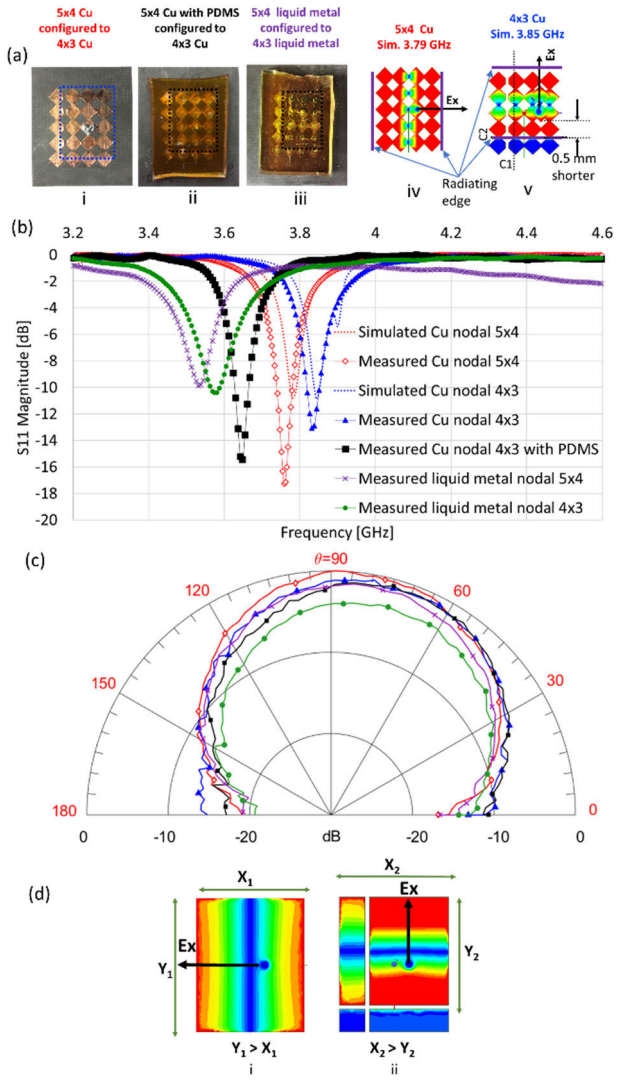

FIGURE 11. Simulated and experimental results for the 4 × 3 Cu and liquid-metal nodal antennas a) i-iii. photographs, iv-v. Simulation of Cu nodal 5 × 4 and 4 × 3 antennas showing a switch in polarization; b) $|S_{11}|$; c) radiation patterns for normalized co-polarized H-plane; the legend is the same as that in b); d) A solid patch antenna simulation showing the switch in polarization due to the change in dimension through row and column subtraction.

Disconnecting column 1 and row 5 of the 5 × 4 liquid-metal antenna resulted in a 90° switch in polarization from horizontal to vertical. The 5 × 4 antenna radiation is horizontally polarized and radiates along the longer edges as shown in Fig. 11(a)(iv). However, splitting of the column 1 and row 5 nodes changes the dimension to a 4 × 3 antenna [Fig. 11(a)(v)], resulting in a change in radiation edge and polarization. Although column 1 and row 5 are physically disconnected in Fig. 11(a)(v), the simulation shows that the elements in column 1 are capacitively coupled, creating a virtual 4 × 4 antenna. Column 1 is parallel to the direction of E_x in Fig. 11(a)(v) and shows a similar field distribution to columns 2–4, whereas row 5 is perpendicular to E_x resulting in an E-field null over the nodes in that row. Therefore,

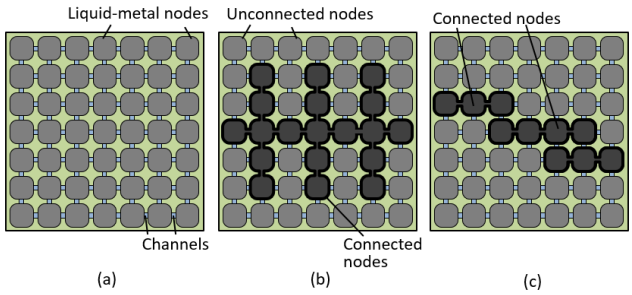

FIGURE 12. Notional example of reconfigurable filter using two-dimensional liquid-metal nodal sheet, showing metal node: (a) unconnected, (b) selectively connected to form a low-pass filter, and (c) connected to form a bandpass filter.

the combined effect of node coupling in column 1 and a null E-field in row 5 causes the horizontal (X_2) edge to be longer, resulting in a polarization switch from horizontal to vertical. The phenomenon is further verified in Fig. 11(d) by simulating a solid Cu patch antenna, where subtracting solid slices that are dimensionally equivalent to one nodal row and one nodal column result in a switch from horizontal to vertical polarization; note that in the horizontally polarized case, $Y_1 > X_1$, whereas in the vertical polarization case, $X_2 > Y_2$. The right side of Table 1 summarizes the antenna performance, with the last row being the most important as it is the only case that allows reversible reconfigurability.

The last row of Table 1 shows that pressure-point merging/splitting is a reversible process which allows the liquid-metal antenna to switch between horizontal and vertical polarizations, without an appreciable change in frequency. While it is true that there is a corresponding reduction in gain in switching from 5 × 4 to 4 × 3, each of the rows in Table 1 for the nodal antennas show that there is some reduction in gain, understandable due to the smaller effective aperture. Also, the reduction in gain while switching from Cu to liquid metal is consistent with results we have seen in similar work [25].

The nodal sheet is designed to minimize the effect of gravity on the liquid metal. The diamond-shaped node acts as a tapered channel with sufficient fluidic resistance to stabilize the liquid metal against gravity. Additionally, the notch in each node helps to anchor the liquid metal. The combination of these features prevents liquid metal from connecting to nodes in the bottom row, as shown in Fig. 11(a)(iii); here the antenna is held in a vertical position to take the radiation pattern measurement.

V. CONCLUSION

This article demonstrated a two-dimensional liquid-metal nodal sheet that could be reconfigured by merging and splitting adjacent nodes. Three different actuation schemes were presented, in which reconfiguration occurred on the order of 0.15–1 s. In addition, a proof-of-concept nodal sheet patch antenna was demonstrated, in which the liquid-metal nodes are reversibly connected and disconnected to change

the operating frequency and polarization. The liquid-metal merging/splitting schemes demonstrated in this work could facilitate prototyping of other types of reconfigurable microcircuits, such as a reconfigurable filter (Fig. 12). The work presented here is part of a dissertation containing additional ideas, experiments, and demonstrations [26].

ACKNOWLEDGMENT

The authors would like to thank Matthew Moorefield, Kent Sarabia, Anthony Combs, and Ryan Gough for their support and discussion in the early stages of this work.

REFERENCES

[1] J. C. Lyke, C. G. Christodoulou, G. Alonzo Vera, and A. H. Edwards, "An introduction to reconfigurable systems," *Proc. IEEE*, vol. 103, no. 3, pp. 291–317, Mar. 2015.
[2] D. Rodrigo, B. A. Cetiner, and L. Jofre, "Frequency, radiation pattern and polarization reconfigurable antenna using a parasitic pixel layer," *IEEE Trans. Antennas Propag.*, vol. 62, no. 6, pp. 3422–3427, Jun. 2014.
[3] A. Grau Besoli and F. De Flaviis, "A multifunctional reconfigurable pixeled antenna using MEMS technology on printed circuit board," *IEEE Trans. Antennas Propag.*, vol. 59, no. 12, pp. 4413–4424, Dec. 2011.
[4] D. Rodrigo and L. Jofre, "Frequency and radiation pattern reconfigurability of a multi-size pixel antenna," *IEEE Trans. Antennas Propag.*, vol. 60, no. 5, pp. 2219–2225, May 2012.
[5] M. D. Dickey, "Emerging applications of liquid metals featuring surface oxides," *ACS Appl. Mater. Interface*, vol. 6, no. 21, pp. 18369–18379, Nov. 2014.
[6] J. H. Dang, R. C. Gough, A. M. Morishita, A. T. Ohta, and W. A. Shiroma, "Liquid-metal-based reconfigurable components for RF front ends," *IEEE Potentials*, vol. 34, no. 4, pp. 24–30, Jul. 2015.
[7] K. Entesari and A. P. Saghati, "Fluidics in microwave components," *IEEE Microw. Mag.*, vol. 17, no. 6, pp. 50–75, Jun. 2016.
[8] M. A. Rahman, R. C. Gough, M. M. Moorefield, G. B. Zhang, W. A. Shiroma, and A. T. Ohta, "Electrically actuated liquid metal for reconfigurable RF devices," in *Proc. IEEE/ACES Int. Conf. Wireless Inf. Technol. Syst. (ICWITS) Appl. Comput. Electromagn. (ACES)*, Mar. 2016, pp. 1–2.
[9] D. J. Fisher, *Liquid Metal Alloys in Electronics. Materials Research Foundations*, vol. 70, Millersville, PA, USA: Materials Research Forum, LLC, 2020.
[10] T. Liu, P. Sen, and C.-J. Kim, "Characterization of nontoxic liquid-metal alloy galinstan for applications in microdevices," *J. Microelectromech. Syst.*, vol. 21, no. 2, pp. 443–450, Apr. 2012.
[11] J.-H. So, J. Thelen, A. Qusba, G. J. Hayes, G. Lazzi, and M. D. Dickey, "Reversibly deformable and mechanically tunable fluidic antennas," *Adv. Funct. Mater.*, vol. 19, no. 22, pp. 3632–3637, Nov. 2009.
[12] M. A. Rahman, W. A. Shiroma, and A. T. Ohta, "Liquid-metal capacitors with a 42:1 tuning ratio," *Electron. Lett.*, vol. 53, no. 11, pp. 710–711, May 2017.
[13] R. C. Gough, A. M. Morishita, J. H. Dang, W. Hu, W. A. Shiroma, and A. T. Ohta, "Continuous electrowetting of non-toxic liquid metal for RF applications," *IEEE Access*, vol. 2, pp. 874–882, 2014.
[14] R. C. Gough, A. M. Morishita, J. H. Dang, M. R. Moorefield, W. A. Shiroma, and A. T. Ohta, "Rapid electrocapillary deformation of liquid metal with reversible shape retention," *Micro Nano Syst. Lett.*, vol. 3, no. 1, pp. 1–9, Apr. 2015.
[15] K. J. Sarabia, S. S. Yamada, R. C. Gough, M. R. Moorefield, A. W. Combs, W. A. Shiroma, and A. T. Ohta, "Out-of-plane continuous electrowetting actuation of liquid metal," *Electron. Lett.*, vol. 53, no. 25, pp. 1635–1636, Dec. 2017.
[16] K. J. Sarabia, W. A. Shiroma, and A. T. Ohta, "Pixelated reconfiguration using electrically actuated liquid metal," *Electron. Lett.*, vol. 54, no. 4, pp. 192–194, Feb. 2018.
[17] A. M. Watson, K. Elassy, T. Leary, M. A. Rahman, A. Ohta, W. Shiroma, and C. E. Tabor, "Enabling reconfigurable all-liquid microcircuits via Laplace barriers to control liquid metal," in *IEEE MTT-S Int. Microw. Symp.*, Jun. 2019, pp. 188–191.
[18] A. M. Watson, T. F. Leary, K. S. Elassy, A. G. Mattamana, M. A. Rahman, W. A. Shiroma, A. T. Ohta, and C. E. Tabor, "Physically reconfigurable RF liquid electronics via Laplace barriers," *IEEE Trans. Microw. Theory Techn.*, vol. 67, no. 12, pp. 4881–4889, Dec. 2019.
[19] P. K. Yuen and V. N. Goral, "Low-cost rapid prototyping of flexible microfluidic devices using a desktop digital craft cutter," *Lab Chip*, vol. 10, no. 3, pp. 384–387, 2010.
[20] G. B. Zhang, R. C. Gough, M. R. Moorefield, A. T. Ohta, and W. A. Shiroma, "An electrically actuated liquid-metal switch with metastable switching states," in *IEEE MTT-S Int. Microw. Symp. Dig.*, May 2016, pp. 1–4.
[21] C. B. Eaker and M. D. Dickey, "Liquid metal actuation by electrical control of interfacial tension," *Appl. Phys. Rev.*, vol. 3, no. 3, Sep. 2016, Art. no. 031103.
[22] T. Tanaka, M. Matsuda, K. Nakao, Y. Katayama, D. Kaneko, S. Hara, X. Xing, and Z. Qiao, "Measurement of surface tension of liquid Ga-base alloys by a sessile drop method," *Zeitschrift Füer Met. Res. Adv. Tech.*, vol. 92, no. 11, pp. 1242–1246, 2001.
[23] K. S. Elassy, M. A. Rahman, N. S. Yama, W. A. Shiroma, and A. T. Ohta, "Complex permittivity of NaOH solutions used in liquid-metal circuits," *IEEE Access*, vol. 7, pp. 150150–150156, 2019.
[24] C. A. Balanis, *Antenna Theory: Analysis and Design*, 3rd ed. Hoboken, NJ, USA: Wiley, 2005, pp. 816–843.
[25] K. J. Sarabia, A. T. Ohta, and W. A. Shiroma, "Pixelated dual-dipole antenna using electrically actuated liquid metal," *Electron. Lett.*, vol. 55, no. 19, pp. 1032–1034, Sep. 2019.
[26] K. S. Elassy, "Reconfigurable and flexible liquid-metal devices and circuits," Ph.D. dissertation, Dept. Elect. Eng., Univ. Hawai'i at Mānoa, Honolulu, HI, USA, 2020. [Online]. Available: http://hdl.handle.net/10125/68985

KAREEM S. ELASSY (Student Member, IEEE) received the B.S. and M.S. degrees in electronics and communications engineering from the Arab Academy for Science, Technology and Maritime Transport, Cairo, Egypt, in 2009 and 2014, respectively, and the Ph.D. degree in electrical engineering from the University of Hawai'i (UH) at Mānoa, Honolulu, HI, USA, in 2020.

He is currently a Transistor Integration Engineer at Intel Corporation. In 2013, he joined the Egypt-IBM Nanotechnology Research Center as a Researcher. He worked on a wide spectrum of research projects at the University of California at Berkeley, Berkeley, CA, USA, and the Technical University of Darmstadt, Darmstadt, Germany, in the field of printed electronics.

Dr. Elassy was a recipient of the 2019 Department of Electrical Engineering Research Excellence Award and the 2020 College of Engineering Outstanding Ph.D. Student Award at UH Mānoa. He is also the Chair of the IEEE Microwave Theory and Techniques Society UH Student Branch Chapter.

M ARIFUR RAHMAN (Senior Member, IEEE) received the B.S. degree in naval science from the Bangladesh Naval Academy, Chittagong, Bangladesh, in 2002, the B.S. degree in electrical engineering from the Military Institute of Science and Technology, Dhaka, Bangladesh, in 2006, and the Ph.D. degree in electrical engineering from the University of Hawai'i (UH) at Mānoa, Honolulu, HI, USA, in 2018.

In 2006, he joined the Bangladesh Navy, where he served as a Senior Electrical Engineer in various navy warships and establishments and retired as a Lieutenant Commander, in 2013. He is currently a Postdoctoral Fellow with UH Mānoa. He has authored over 22 publications in the areas of microelectromechanical systems and microfluidics.

Dr. Rahman was a recipient of the 2018 UH Mānoa College of Engineering Outstanding Ph.D. Student Award. He is currently the Vice Chair of the IEEE Microwave Theory and Techniques Society Hawai'i Chapter, the Chair of the IEEE Young Professionals Hawai'i Chapter, and a member of the Electronic Product and Services Board for the IEEE Robotics and Automation Society.

WAYNE A. SHIROMA (Senior Member, IEEE) received the B.S. degree from the University of Hawai'i (UH) at Mānoa, Honolulu, HI, USA, in 1986, the M.Eng. degree from Cornell University, Ithaca, NY, USA, in 1987, and the Ph.D. degree from the University of Colorado at Boulder, Boulder, CO, USA, in 1996, all in electrical engineering.

In 1996, he joined UH Mānoa, where he is currently a Professor and the Department Chair of electrical engineering. He was also a member of the Technical Staff at Hughes Space and Communications, El Segundo, CA, USA. He has authored over 130 publications in the areas of microwave circuits and antennas, nanosatellites, and engineering education.

Dr. Shiroma served three terms on the IEEE Microwave Theory and Techniques Society (MTT-S) Administrative Committee, from 2002 to 2010, was the General Chair of the 2007 and 2017 IEEE MTT-S International Microwave Symposiums, and received the IEEE MTT-S Distinguished Service Award in 2019. He was a recipient of the 2003 UH Regents' Medal for Excellence in Teaching, the ten-campus UH System's most prestigious teaching award. Since 2001, IEEE-HKN, the international honor society for IEEE, recognized four of his graduating seniors as the most out-standing electrical engineering students in the U.S.

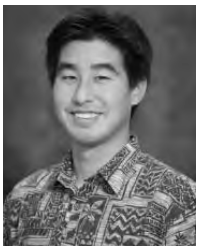

AARON T. OHTA (Senior Member, IEEE) received the B.S. degree from the University of Hawai'i (UH) at Mānoa, Honolulu, HI, USA, in 2003, the M.S. degree from the University of California at Los Angeles, Los Angeles, CA, USA, in 2004, and the Ph.D. degree from the University of California at Berkeley, Berkeley, CA, USA, in 2008, all in electrical engineering.

In 2009, he joined UH Mānoa, where he is currently a Professor of electrical engineering. He has authored over 130 publications in the areas of microelectromechanical systems and microfluidics.

Dr. Ohta was a recipient of the 2012 UH Regents' Medal for Excellence in Research, the 2015 UH Regents' Medal for Excellence in Teaching, the ten-campus UH System's most prestigious research and teaching awards, respectively. He is also an Associate Vice President of the IEEE Robotics and Automation Society's Technical Activities Board.